PERGAMON

Journal of Asian Earth Sciences 21 (2002) 265–282

Journal of Asian Earth Sciences

www.elsevier.com/locate/jseaes

Geology, geochemistry and Ar–Ar geochronology of the Nangimali ruby deposit, Nanga Parbat Himalaya (Azad Kashmir, Pakistan)

A. Pêcher[a,*], G. Giuliani[b], V. Garnier[c], H. Maluski[d], A.B. Kausar[e], R.H. Malik[f], H.R. Muntaz[f]

[a]*LGCA, OSUG, Maison des Géosciences, 1381 rue de la Piscine, BP 53, 38031 Grenoble, France*
[b]*IRD and CRPG/CNRS, UPR 2300, BP 20, 54501 Vandœuvre, France*
[c]*CRPG/CNRS, UPR 2300, BP 20, 54501 Vandœuvre, France*
[d]*Laboratoire de Géochronologie, Université de Montpellier 2, Place Eugène Bataillon, 34095 Montpellier, France*
[e]*GSP, Geoscience Laboratory, P.O. Box 1461, Shahzad Town, Islamabad, Pakistan*
[f]*AKMIDC, P.O. Box 8, Muzaffarabad, Azad Kashmir, Pakistan*

Received 23 July 2001; revised 15 March 2002; accepted 25 April 2002

Abstract

The Nangimali ruby deposit in the southern part of the Nanga Parbat Himalaya, has been investigated through field work, geochemistry, stable and radiogenic isotopes. It outcrops in the Shontar valley in a large north-vergent syncline consisting of high-grade metamorphic gneisses capped by a metasedimentary series dominated by marbles and amphibolites. The ore-body is stratiform. Ruby is found within 0.1–2 cm thick shear-veinlets and gash veins cutting dolomitic marbles and carbonate-bearing bands.

The marbles of the Nangimali Formation display restricted ranges in $\delta^{18}O$ (from 23.6 to 27.6‰ relative to SMOW) and in $\delta^{13}C$ (from −1.9 to 2.6‰ relative to PDB). Fluid infiltration along the shear-zone in the marble has no effect on the isotopic signatures of the carbonates. Fluids are metamorphic and CO_2 is derived from the decarbonation of marbles.

Mass-balance and geochemical analyses suggest that the mobilisation by the fluids of aluminium and chromium in the marbles is sufficient to enable the formation of ruby in the shear-zone. Rubies have been indirectly dated using a stepwise ^{40}Ar–^{39}Ar laser heating technique on syngenetic phlogopites. The Miocene age records a Neogene cooling in the South of the Nanga Parbat massif and a minimum formation age for ruby of 16 Ma.

Keywords: Geology; Geochemistry; Stable isotopes; Ar–Ar geochronology; Phlogopite; Ruby deposit; Himalaya; Nangimali; Azra Kashmir; Pakistan

1. Introduction

The Nanga Parbat–Haramosh massif, a north–south elongated spur of gneisses and cover sequences, is located at the north-west end of the Himalayas, in the core of the western syntaxis of the belt. The northern and central part of the massif has been extensively studied during the past few years, as demonstrated by the extensive references in Treloar et al. (2000a) and Edwards et al. (2000). Limited to the West, North and East by the large remnants of the Cretaceous Kohistan–Ladakh volcanic arc, the massif represents an exhumed half window of Indian continental basement. The northern part, the Indus valley section, corresponds to a crustal scale north–south trending anticlinorium (Coward et al., 1986; Seeber and Pêcher, 1998). Farther to the South, in the Nanga Parbat summit section, it evolves to a doubly vergent pop-up structure pinched between two large mylonitic zones, the Diamir shear-zone at West and the Rupal shear-zone at East (Schneider et al., 1999a; Fig. 1). The dominant lithological components are the migmatitic Nanga Parbat gneisses (Wadia, 1933; Mish, 1949).

Farther South, both sides of the Nanga Parbat spur, the contact between Himalayan gneiss and Kohistan–Ladakh arc formation (the Main Mantle Thrust, MMT), is again parallel to the general NE–SW trend of the belt. The western part of this zone, between MMT and southern prolongation of the Diamir shear-zone, has been the object of detailed studies, but the south-eastern termination of the Nanga Parbat spur, in the upper Neelum valley close to Kashmir border, is still poorly known. Most of the available data are synthesised in Azad Kashmir Mineral and Industrial Development Corporation (AKMIDC) unpublished reports

* Corresponding author. Tel.: +33-476-514-108; fax: +33-476-514-058.
E-mail address: arnaud.pecher@ujf-grenoble.fr (A. Pêcher).

1367-9120/02/$ - see front matter © 2002 Elsevier Science Ltd. All rights reserved.
PII: S1367-9120(02)00041-X

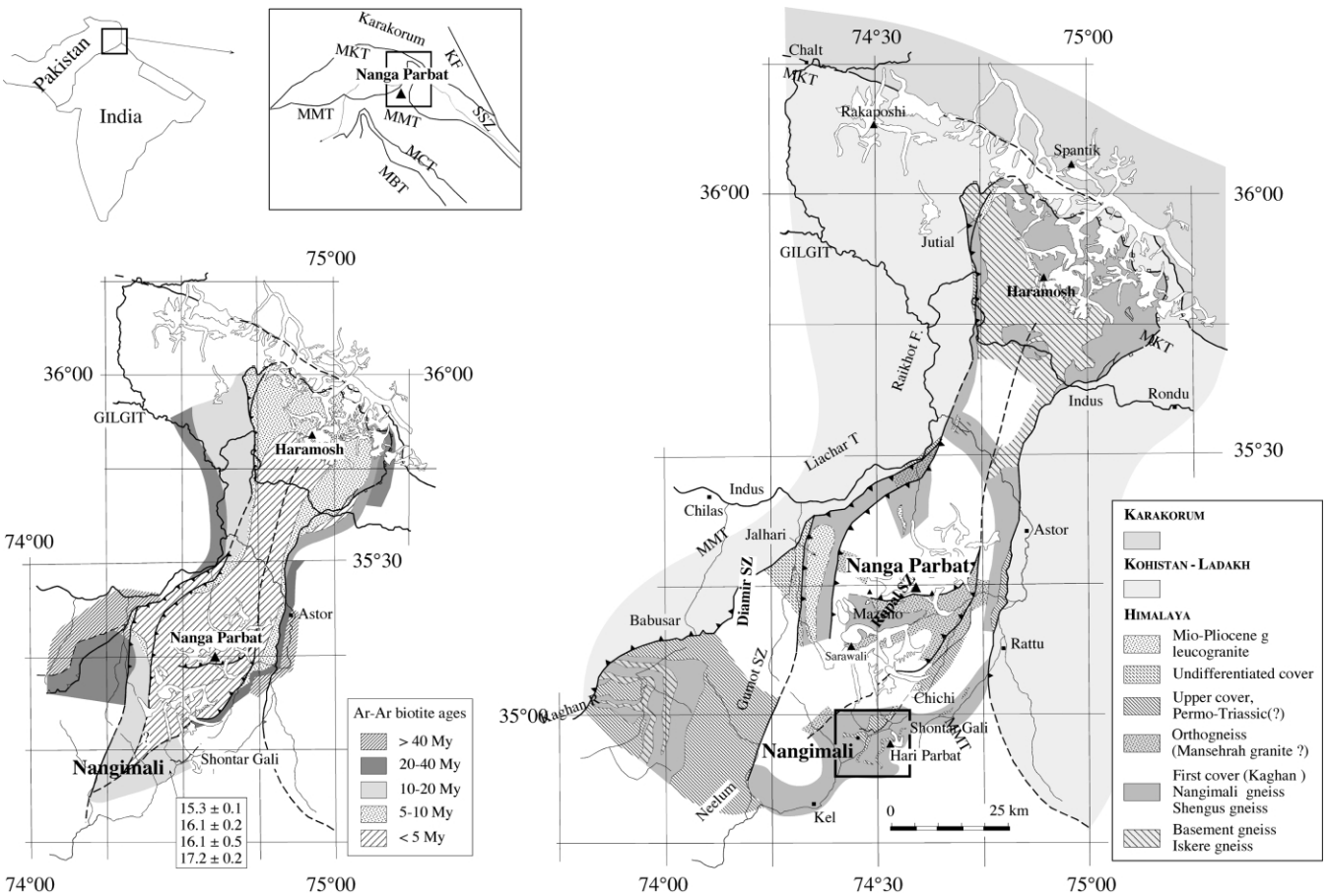

Fig. 1. The Nanga Parbat–Haramosh spur. Right: geological map. Nanga Parbat area from Edwards et al. (2000), Schneider et al. (1999c) and Edwards and Kidd (personal communication); Babusar and Kaghan area from Lombardo and Rolfo (2000); Gumot shear-zone from Malik et al. (1996). Left: repartition of $^{40}Ar/^{39}Ar$ cooling ages on biotite across the spur. Data from Treloar et al. (2000a), Schneider et al. (1999b,c, 2001). Nangimali ages: this paper.

by Malik (1994) and Malik et al. (1996). In this area, AKMIDC is currently mining several ruby deposits, the main one being located close to Nangimali summer settlement. The following report provides additional geological, geochemical and radiometric data resulting from new field work and sampling in the Nangimali area, and mapping of the upper Neelum valley and Shontar Gali pass area.

2. Geological framework

In the northern Nanga Parbat area, Himalayan formations chiefly consist of imbricated high-grade orthogneisses and metavolcanic and metasedimentary paragneisses (Madin, 1986; Madin et al., 1989), possibly with a 'basement-cover' relationship (Treloar et al., 1991). The rocks had a long metamorphic history: the metamorphic fabric predates a suite of amphibolitic dykes that have been dated at 1.8 Ga (an Sm–Nd isochron age of Butler et al. (1992) and Treloar et al. (2000b)), but the peak thermal event would be younger than 45 Ma (Chamberlain and Zeitler, 1996). In rocks from the Indus Gorge, hornblende Ar/Ar ages are in the range 28–21 Ma, and most biotite cooling ages are younger than 10 Ma (Treloar et al., 2000a; Schneider et al., 2001).

The region farther south, around the Nanga Parbat summit, is the location of many recent studies (Treloar et al., 1991, 2000b; Schneider et al., 2001; Argles, 2000; Butler et al., 1989, 2000; Edwards et al., 2000). Here, the core of the massif is composed of similar migmatitic orthogneisses and felsic metasedimentary paragneisses, flanked to the east and west by a series of less metamorphosed, non-migmatised, metasedimentary outcrops. These series (Upper Cover, Edwards et al., 1997, 2000, or Tarshing series, Butler et al., 2000; Argles, 2000) are composed of pelites, psammites, interbedded calcshists or marbles, associated with amphibolites. They can be clearly distinguished from the central migmatitic gneisses, where carbonate-bearing rocks are nearly totally absent. For Treloar et al. (2000a) and Edwards et al. (2000), the Upper Cover is probably a metamorphic equivalent of the Upper Paleozoic–Lower Mesozoic platform cover of the Himalayas. The amphibolite–marble association would correspond to the Permian Panjal Traps, which comprise mafic sills or flows interbedded in the carbonate platform of the Indian margin.

In the Nanga Parbat area, the early metamorphic events are nearly completely obliterated by Late Miocene and younger high-grade amphibolite to granulite-facies metamorphism and anatexis, followed by extremely rapid cooling and exhumation (Smith et al., 1992; Zeitler et al., 1993; Winslow et al., 1995). Basement cooling ages and the intrusive ages of leucogranites become younger from North to South (from 9.5 Ma for the Jutial granite North of the Indus section, to 1.4 Ma for the Mazeno pass granite on the Nanga Parbat transect, see Schneider et al. (1999b) and Schneider et al. (2001)). This transition is explained in terms of exhumation of the innermost core of the massif, in parallel to an accentuation of its overall pop-up shape.

The Nanga Parbat pop-up is bounded by two broad ductile shear-zones, marked by penetrative S–C and stretching fabrics (Schneider et al., 1999a; Edwards et al., 2000). The Eastern zone splits in two branches in the Rupal area. The northern branch, which bends east–west South of Nanga Parbat summit, is a thrust that transported to the South the migmatitic gneisses above the non-migmatitic metasediments of the upper cover (Butler et al., 2000). The other branch, which strikes NNE–SSW, is underlain by a kilometre-wide sheared granitic orthogneiss. Farther South, in the Chichi valley, this shearing affects the cover rock sequence. To the South (only 10–15 km north of Nangimali area), the cover is intruded by the Chichi leucogranite, whose position relative to the shear deformation is unclear. However, the Th–Pb age of this rock is between 22 and 16 Ma (Schneider et al., 1999c) and this date provides evidence of an Early Miocene thermal event in Southern Nanga Parbat.

To the West, opposite the Rupal shear, the Diamir shear-zone (Edwards et al., 1997; Schneider et al., 1999a; Edwards et al., 2000; DiPietro et al., 2000) is marked by granitic gneisses with a steep east-dipping shear fabric, passing westwards to the non-deformed Jalhari biotite granite, which intruded at 13 Ma synchronously with the ductile deformation (Schneider et al., 1998; Schneider et al., 1999a). Biotite cooling ages in the hanging-wall of the shear-zone are less than 5 Ma old, while in the foot wall, they are older than 20 Ma (Schneider et al., 1999a). The Gumot shear-zone, mapped by Malik et al. (1996), appears to be the Southern prolongation of the Diamir shear.

Most studies of the geology of Himalayan formations south of Nanga Parbat have focussed on the Kaghan valley area, between the MMT and the Gumot shear-zone. West of the Nanga Parbat pop-up corner, the MMT can be followed south of Babusar Pass along the western side of the Kaghan valley. Its movement involved SW-directed thrusting before 40 Ma, associated with amphibolite-facies metamorphism in Himalayan formations, then SE-directed thrusting between 40 and 25 Ma (Chamberlain et al., 1991). In the foot wall, the crystalline core of the Higher Himalayas has been separated by Greco et al. (1989) into two main divisions: basement and cover. As elsewhere in Nanga Parbat, the basement is composed of gneisses (predominantly augen orthogneisses) and pelitic metasediments (the Naram formation of Greco et al. (1989); or the Bhurjanwali formation of Hashmi et al. (1990); in Malik (1994)). For Greco et al., the basement orthogneisses probably correlate with Cambrian Mansehra type granites in the Lesser Himalayas. The Naram formation, which forms a sheet above the gneisses, could represent a Lower Paleozoic sequence, the 'Lower Cover' of Spencer et al. (1990). These units are followed by a more diverse cover series, referred to by Greco et al. (1989) as simply the 'cover sequence', or by Spencer et al. (1990) as the 'Upper Cover' or 'second cover'. This sequence comprises lower amphibolite unit overlain by marbles, calcareous mica-schists and intercalated sheets of amphibolite. According to Papritz and Rey (1989) and Spencer et al. (1995), the amphibolites closely resemble, both petrographically and geochemically, the Permo-Triasic Panjal Traps, or rather their metamorphic equivalents as described in the Suru Valley (Zanskar) by Honneger et al. (1982) and Honneger (1983). Still higher in the sequence, the Parla Sapat unit, which is pinched directly below the MMT, is composed of graphitic garnet and staurolite-bearing mica-schists and minor marbles. This unit has been compared with the Mesozoic Saidu formation, in the Swat area, farther to the West (Khan et al., 1995).

Particularly noticeable in the Kaghan area are remnants of HP rocks in the Himalayan gneiss: glaucophane and barroisite-phengites eclogites, have been found in several localities (Chaudry and Ghazanfar, 1987; Spencer et al., 1990; Pognante and Spencer, 1991; Pognante, 1992). According to Lombardo et al. (2000) and Lombardo and Rolfo (2000), they record peak metamorphic temperatures of 580–600 °C and pressures greater than 23–24 kb. Very high pressures are recorded in a recent discovery of coesite-bearing rocks (O'Brien et al., 2001) that formed at more than 27 kb and 690 °C.

East of the Kaghan valley, the geology of the right flank of the Neelum valley, from the Lesser Himalayas up to Nangimali, is described by Malik et al. (1996). The formations of the Higher Himalayas are subdivided into three main litho-stratigraphical groups: (1) the Precambrian Naril group, composed of granulitic gneisses, is equivalent to the basement gneisses of the Kaghan valley, (2) the pelitic and psammatic metasediments of the Kundalshahi group, also called the Prehimalayan cover, for which a Precambrian–Cambrian age is suggested, are similar to the Naram group (Lower Cover) of Kaghan valley, and (3) the Surgun group, which is mainly characterised by the abundance of paragneisses and marbles, is analogous to the Kaghan Upper Paleozoic–Mezosoic Upper Cover. Both the Naril group and Kundalshahi groups are intruded by Cambrian Mansehra type granitic intrusions, which outcrop as large patches of orthogneiss. The cover series (Surgun group) are said to be Triassic to Middle Jurassic, based on comparison with similar series not far to the South, from the dating by fossils in similar formations of the Lesser

Himalayas (Malik et al., 1996), and by comparison with the Permo-Triasic Panjal Traps.

Fig. 1 is a new tentative lithological map of the Nanga Parbat–Haramosh region, prepared on the basis of the information summarised earlier, and including our new data in the Nangimali area. The principal uncertainties concern (a) the real nature of the basement-cover relationship north of Astor valley, (b) the distinction between Cambrian (Mansehra type) orthogneisses and Proterozoic basement orthogneisses, (c) possible confusion between the Prehimalayan Cover and either the basement gneisses or the Permo-Triasic Upper cover, and (d) the actual stratigraphical ages.

3. Geology of the Shonthar Nala valley, around the Nangimali area

3.1. Lithology

Preliminary geological mapping has been conducted along Shonthar Nala (the main northern tributary of the upper Neelum River, Fig. 2), upstream from Tardi Domel to the Shontar Gali pass, and along its main tributaries (Bundar Nala, Lunda Nala, Mohri Nar, Chitta Katha Nala and northern glacier of Hari Parbat summit). Additional information has been also collected on the northeastern side of the Shontar Gali (Shontar pass), on the way down to Rattu along Mir Malik stream, a southern tributary of the Astor river.

Strong contrasts between massive, homogeneous felsic gneisses, and a heterogeneous, predominantly calcareous, cover series mark the landscape. The calcareous units are exposed in kilometre-size synforms (Nangi Mali and Khundi Gali synclines), in pinched remnants of fold hinges (Shontar Gali area), and in interfoliated thin bands that do not exceed a few hundred metres in thickness but follow for the main units for more than 10 km (western and northern slopes of Hari Parbat).

In the gneissic series, two main types of gneisses are encountered (i) feldspar- and quartz-rich biotite paragneisses, often slightly migmatitic, and (ii) homogeneous orthogneisses. The latter are leucocratic coarse-grained metagranites, often porphyritic. When observed, the contact with paragneisses is sharp; the orthogneisses resemble large laccolithic-shaped intrusions. Although no age data are available on these gneisses, a correlation with Cambrian (516 Ma, Le Fort et al., 1980) Manserah-type granites seems evident. According to Malik et al. (1996), the paragneisses form part of the so-called ‘Prehimalayan cover’ (Kundalshahi group) rather than the basement Naril group. Actually, the homogeneity of the gneiss encountered in the Shonthar Gali area is in marked contrast to the heterogeneity of the Kundalshahi group as previously described, and the exact affiliation of those gneisses, as well as their approximate age, remains debatable.

Metamorphism was in the upper amphibolite facies, as indicated by the paragenesis muscovite + biotite + garnet ± kyanite. In Lunda Nala and Chitta Katha Nala, kyanite + light coloured epidote (zoisite ?) is found, suggesting higher pressures. Altered cordierite has been found in one location in Lunda Nala, and sillimanite is known a little further west, in the Chatthewala area (Malik et al., 1996).

In Nangimali and surroundings area (from Shontar Gali Pass up to the MMT and down the Rattu valley), the gneisses are capped by metasedimentary formations with interbeds of aluminous metapelites, phlogopite-rich brownish calcshists, quartzites, bands of white marbles and thin (less than 100 m) bands of amphibolites. This cover sequence, which contains several ruby deposits, has been studied and described in detail by AKMIDC geologists. The litho-statigraphic series given in Fig. 3 (modified from Malik (1994)) corresponds to the reverse limb of the Nangimali syncline in the Lower Korat mining area.

Particularly notable is the amphibolite–marble association, which is fairly similar to the Panjal Trap Permo-Triassic sequence found on the other side of the broad Kashmir syncline, in the Zanskar area; its tectonic setting is also very similar, in the core of tight synmetamorphic isoclinal syncline that folded both the cover and the underlying migmatitic gneisses (Honegger et al., 1982).

3.2. Structure

The upper Shontar Nala valley is dominated by the two broad isoclinal synclines of Nangimali and Khundi Gali, which refolded both the foliation of the basement gneiss and contacts with sedimentary units (Fig. 2).

The main Nangimali syncline, which can be followed between 2800 m in the valley up to 4600 m on the ridge, is almost entirely pinched between its two gneissic limbs in its upper part, but is much broader in its hinge zone further down the valley. Its upper (reverse) limb is rather regular and in this limb, the gneiss-metasediment contact is parallel to the gneissic foliation. The metamorphic foliation observed in the sediments, manifested mainly by phlogopite orientation (Fig. 4(A)), is generally very close to the stratigraphical bedding, except in the hinge of minor drag-slip type folds, where it defines the axial plane foliation (Fig. 4(B)). At the scale of the bulk structure, the main amphibolite layer is folded into a regular syncline whose axis plunges rather steeply to the southeast. On the other side of the Shonthar valley (the left bank of the Chitta Katha river), numerous tight folds in the quartzitic and marble layers correspond to disharmonic folding in the hinge of the main structure. Measurements of stratigraphic bedding (Fig. 2, stereogram), mainly at the Lower Khora level, define an axis with a strike of 119°E and plunging 35°ESE; the axial plane of the fold, as defined by the average orientation of the phlogopite-bearing schistosity, is oriented at 069°E and dips 46°SE (a north-facing fold).

In the cliff below Khora mine, a fold interference pattern

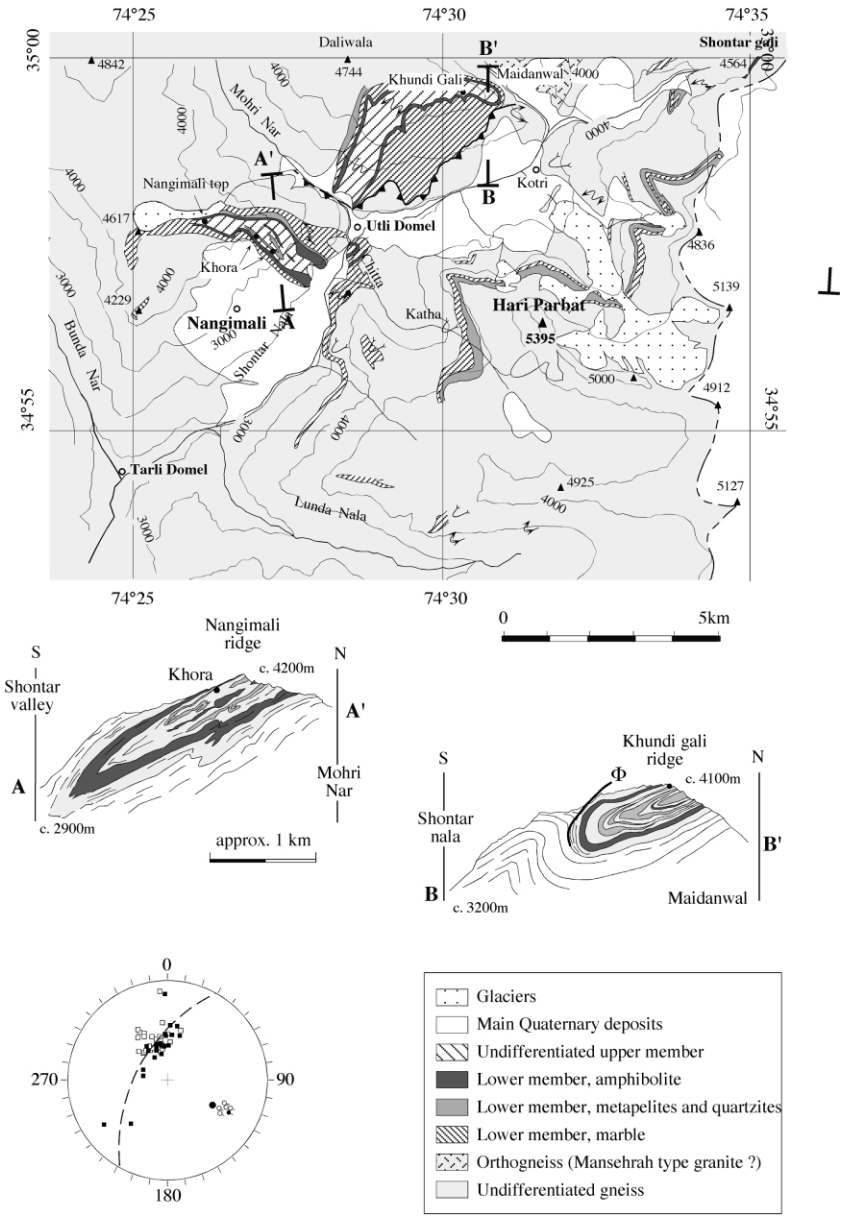

Fig. 2. Geology of Nangimali area. *Geological sketch map*: contours lines every 500 m. Black dots: main ruby deposits. *Nangimali and Khundi Gali sections*, sketched from field photos. Gneisses are in white, marbles in light gray, amphibolites (upper part of the Nangimali Formation lower member) in dark gray, metapelites, quarzites and brownish limestones in medium gray. *Determination of the Nangimali synform axis*. Wulff equiangular projection, lower hemisphere. Black squares: stratigraphical bedding; plain squares: metamorphic foliation; black circles: axis of synmetamorphic fold; plain circles: bedding-foliation intersection lineation. The calculated axis of the synform (pole of the great circle best fitting the bedding and foliation poles) is 119°E, plunging 35°ESE; it lies close to the axis of the small syn-metamorphic secondary folds.

is visible, particularly in banded yellow and white marbles (section A, Fig. 2). It resembles the complicated interference pattern between D1 and D2 Himalayan folds described further West in Neelum valley by Malik et al. (1996). But there the folds are south-vergent, while in Nangimali area, all the structures are north-vergent. Another point to be stressed is the difficulty in defining an accurate stratigraphic section for the upper part of the Nangimali cover series, due to these fold interferences.

North-east of the Nangimali synform, and structurally below it, the spectacular Khundi Gali syncline is the other salient feature of this area. This fold, which is best observed from Maidanwal settlement (Fig. 2, map and section B), is a kilometre-wide concentric structure, developed in the cover series, and relayed to the south by a large anticline in the gneisses. The syncline can be followed along strike some 4 km to WSW, to the Mohri Nar valley. In its central part (at the Kundi Gali crest, where a ruby deposit is known in same structural position as the Nangimali deposits), and farther west in Mohri Nar valley, several hectometric scale secondary disharmonic folds have been observed; in Mohri Nar valley, possibility of earlier D1 folds cannot be

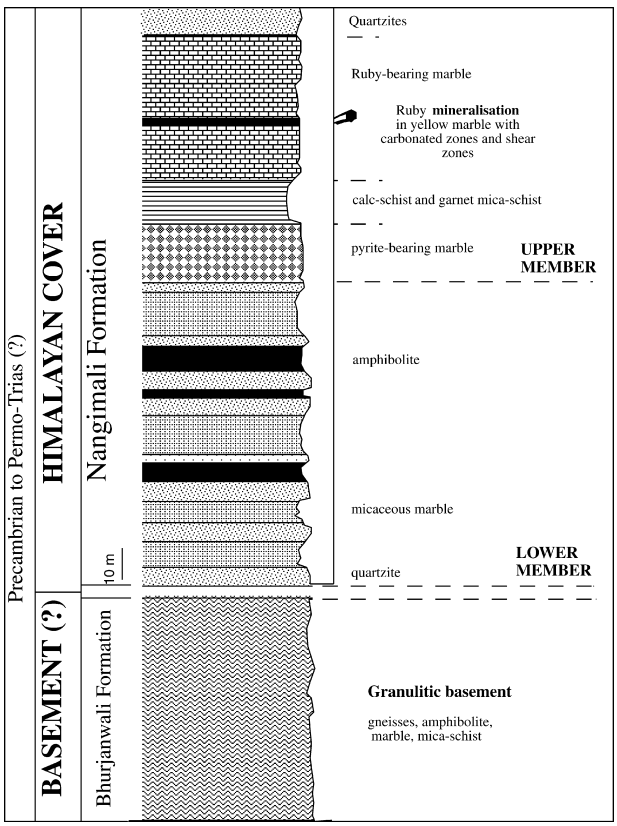

Fig. 3. Nangimali type series, modified from Malik (1994). The litho-stratigraphical attributions remain doubtful. Following Malik (1994), the Nangimali Formation could instead belong to the Paleozoïc 'Prehimalayan cover'. If it is actually Permo-Triasic (Upper cover), as suggested here, then assignment of the whole pile of gneiss to the basement might be wrong.

excluded. In a parallel manner, the gneiss/cover contact of the southern reverse limb evolves from East to West in a top-to-the North thrust.

From cartographic drawing, the orientation of the fold axis is 055°E, and its plunge is at least 20° to the WSW. From direct field measurements, the fold axis is oriented 042°E and dips 19°SE in Khundi Gali and turns to approximately 030°E above Mohri Nar valley. The average bedding plane strikes 061°E, and dips 042° to the SSE. Thus, the two Nangimali and Khundi Gali folds share similar axial-plane directions and a similar northward sense of vergence, but their axes plunge to the SE and SW, respectively. This geometry is best explained by heterogeneous deformation during general northward shearing.

Apart from the two main synclines, several smaller north-vergent isoclinal folds (or remnants of now eroded larger folds) have been observed up to the Shonthar Gali Pass, approximately along the strike of the Nangimali syncline and structurally above the Khundi Gali syncline. These folds probably correspond to the northeastern extension of the Nangimali structure. We have not followed in detail the structural pattern to the East of the main ridge (Shuntar Gali and Chichal Gali), but similar folds can be traced up to Mir Malik, approximately 15 km upstream of Rattu, very close to the MMT.

South of the folded area, the gneissic sequence appears roughly monoclinal, striking WSW–ENE and gently dipping to the South. In places (East of Kotri and in middle Chitta Katha valley, Fig. 2), the sequence is refolded by broad gentle EW post-metamorphic folds; and it is disrupted in its medium part by a continuous band of limestones and aluminous garnet-rich schists. Only the lower contact of this band has been reached, East of Kotri settlement and in the Chitta Katha valley. In both places, the gneiss-metasediments contact is sharp but continuous and apparently was not reactivated tectonically. At both places, the series shares the following features with the Nangimali series: interbedding of aluminous metapelites, phlogopite-rich brownish calcshists, and thin levels of amphibolites and marbles that contain some rubies (H.R. Muntaz). Accordingly, this band appears not to be part of the gneissic pre-Himalayan cover (Kundalshahi formation) but is better interpreted as the Permo-Triassic (?) cover preserved in a highly pinched synform. Its upper contact was not observed; according to R.H. Malik (personal communication), it could be a thrust contact analogous to, but larger than, the reverse-thrusted limb of the Khundi Gali syncline.

4. Nangimali ruby deposits

Ruby in the Nangimali area was discovered in boulders by geologists of the AKMIDC in 1979. Detailed geological investigations were carried out between 1988 and 1994 in the Shontar area. The primary ruby occurrences were discovered at the Nangimali locality and investigated at two locations: Nangimali Top and Khora (Fig. 2). Three years of pilot small-scale mining yielded an ore grade of 11 g/t and the production between 1990 and 1994 was 69 kg of rough ruby for 4 months of production/year (Malik, 1994). The ruby zone is exploited preferentially in benches (Lower Khora, Middle Khora and Nangimali Top) and now in level and adit (Lower Khora mine). The crystals recovered from the different mining zones vary in weight between 0.1 and 40 g. Generally, the ruby crystals have scalenohedral habits up to 5 cm long with sections up to 1 cm in width. The colour of ruby varies from pink to pinkish red (called fancy sapphires) to deep red (called ruby of pigeon blood red, which forms 20% of the whole production).

Ruby mineralisation is hosted by yellowish and grey marbles of the Nangimali Formation over an area of 1.8×0.5 km, from Khora in the east to Nangimali Top in the west. The ore-body refers to several grey carbonate-bearing bands, parallel to the bedding of the Nangimali series (N79°E–41°ESE) and to micro-scale shear-zones, parallel or slightly discordant to the regional foliation and the carbonate-bearing bands (Fig. 4(C) and (D)). The thickness of the bands varies from less than 1 to 30 cm and the total thickness of the different bands can reach several

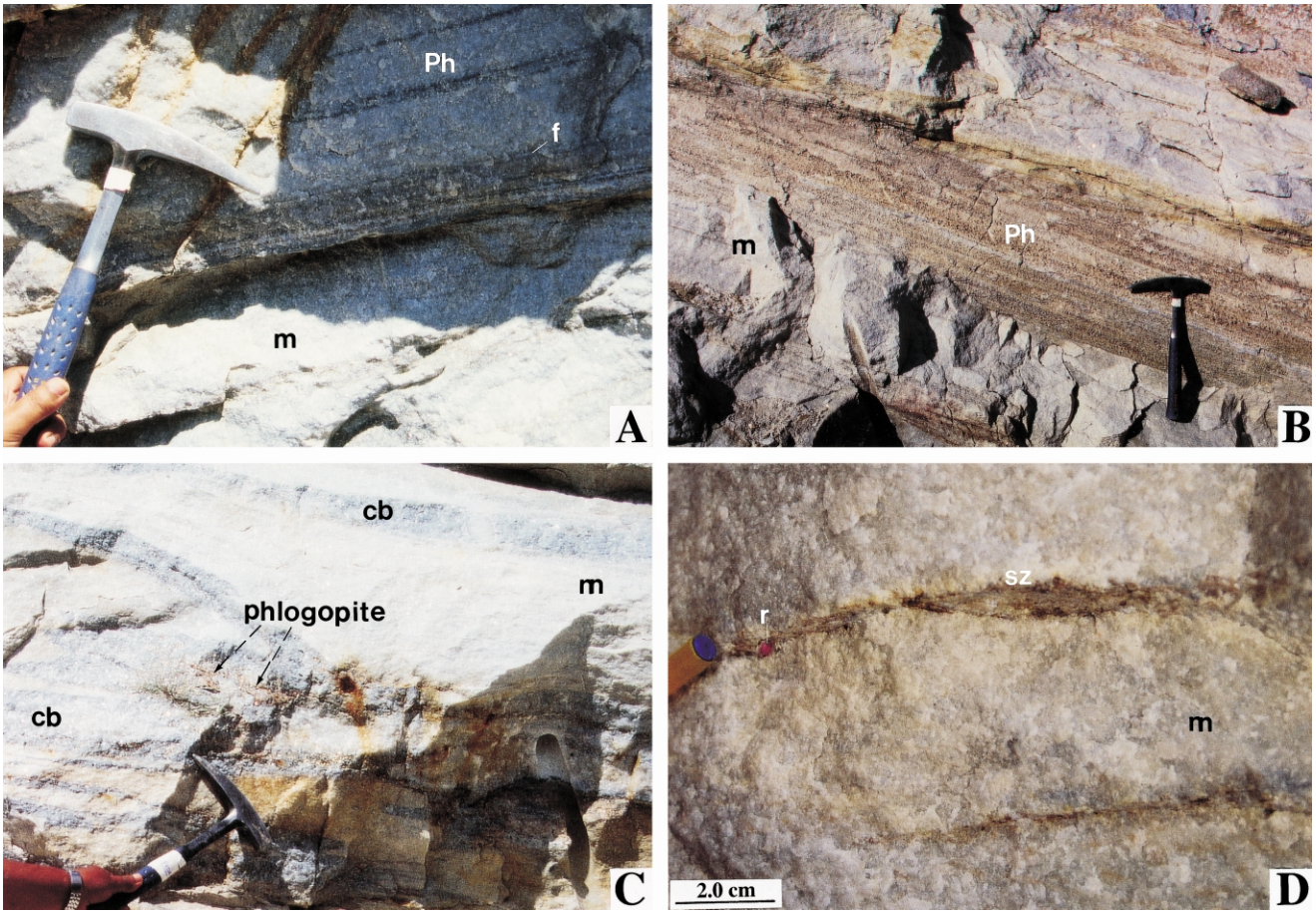

Fig. 4. Photographs of outcrops in the Upper Member of the Nangimali Formation (Khora area) used for dating phlogopite by the $^{40}Ar-^{39}Ar$ method. (A) A pyrite–phlogopite-bearing marble (type c) from the pyrite-bearing marble unit. The pyrite and phlogopite association (Ph) underlines the metamorphic foliation (f) of the marble (m). (B) Phlogopite–pyrite bands (Ph) developed in the yellowish marble (m), parallel to the metamorphic foliation. Note the presence of micro-scale shear-zones that crosscut the phlogopite-rich bands. (C) Phlogopites crystallised in the axis of secondary folds, which affect carbonate-bearing bands (cb) in the yellowish marbles (m). (D) micro-shear-zones (sz) with ruby (r) and phlogopite affecting the yellowish marble (m) in Lower Khora mine.

metres, respectively, 3 m at Khora and 6 m at Nangimali Top. The carbonate-bearing bands are irregular in length and depict pinch and swell structures. The shear-zone system is characterised by 0.5–2 cm thick veinlets or gash veins composed of pyrite ± phlogopite ± rutile ± margarite ± ruby ± pargasite and carbonate.

Ruby deposits in Nangimali have been investigated by geochemistry, stable and radiogenic isotopes in order to better understand their genesis and to obtain constraints on the structural, metamorphic and fluid circulation of the area within the Nanga Parbat framework evolution.

4.1. Analytical methods

A study of the major and trace elements was carried out on the various lithologies of the Nangimali area, with special emphasis on the marble unit. Major- and trace-element concentrations were determined by ICP-MS on 26 representative samples of marbles and schists (Laboratory SARM, CRPG/CNRS, Vandœuvre). In marbles, Al_2O_3 was analysed by absorption spectrometry (1 g of powder/analysis) and TiO_2 by colorimetry after complete calcination and dissolution (1 g of powder/analysis).

Several carbon and oxygen isotopic analyses of marbles were realised. Carbon dioxide was extracted from powdered calcite for dolomite-free marbles by reaction with H_3PO_4 at 25 °C over 3 h, and from powdered calcite–dolomite mixtures for dolomitic marbles by reaction at 50 °C for at least 3 days (McCrea, 1950). The carbon dioxide extracted was analysed by mass spectrometry in a VG 602D mass spectrometer.

Graphite was prepared for carbon isotope measurement by taking 1–2 mg of crystals in the marble and subsequent combustion with excess CuO and Cu_2O, at 900 °C, over 3 h. The carbon dioxide was extracted by cryogenics and analysed by mass spectrometry for carbonates.

$^{40}Ar/^{39}Ar$ has been done on four phlogopite-bearing rocks. Phlogopite grains were separated from the pyrite-bearing and ruby-bearing marbles of the upper member of Nangimali Formation. For laser analyses, single grain samples were wrapped in pure Al-foil packets, loaded in the can as superposed layers, each of them containing a

monitor. Irradiation was carried out in the MacMaster Reactor in Ontario (Canada) for 70 h using fast neutrons. Single grain analysis was carried out using a LEXEL 3500 continuous 6 W argon–ion laser for stepwise heating equipped with a Nier source and a JOHNSTON MM1 electron multiplier for the mass analysis. The five argon isotopes were measured with a MAP 215-50 mass spectrometer at the University of Montpellier (France). Age calculation was done using constants recommended by Steiger and Jäger (1977) and McDougall and Harrison (1988).

4.2. Geochemistry of the marbles and schists in the Upper Member Nangimali Formation

Five types of marbles are distinguished by their mineralogy and geochemistry (Table 1).

In the central and upper parts of the pyrite-bearing marble unit, three types of marbles are found:

- *type* (*a*) corresponds to greyish coarse-grained marble containing pyrite and sometimes graphite. MgO contents are between 2.4 and 6.5 wt%, CaO contents between 47 and 51 wt% and SiO_2 up to 3.8 wt%. The concentration in vanadium is between 5.7 and 21.4 ppm and chromium between 6.9 and 19.1 ppm. Titanium is between 125 and 800 ppm and aluminium between 0.22 and 1.44 wt%.
- *type* (*b*) is a white coarse-grained marble in alternation with type (a). Marbles have MgO contents lower than 1.3 wt% and calcite is coarsely recrystallised. They are depleted in titanium and aluminium. Vanadium and chromium are lower than 10 ppm (Table 2).
- *type* (*c*) is a greyish fine-grained phlogopite–pyrite-bearing impure marble characterised by the alternation of fine bands of pyrite–phlogopite with carbonates, parallel to the foliation. They are Mg–Si–Al-rich; generally, these marbles have MgO contents between 4 and 12.7 wt%. SiO_2 is between 6.1 and 12.4 wt%. They are also enriched in Al_2O_3 with concentrations up to 4 wt%. Vanadium is between 29 and 45 ppm, Cr between 30 and 33 ppm and Ti between 1800 and 2000 ppm (Fig. 5).

The ruby-bearing marbles are composed of two main types:

- *type* (*d*) is a yellowish to white medium- to fine-grained marble. In the field, it presents a yellow colour due to superficial weathering. It corresponds to a Mg-rich dolomitic marble (Figs. 6 and 7(C)) with MgO contents higher than 18.7 wt% (Table 1). Magnesian marbles are alkali-depleted compared to the other types of marbles found in Nangimali. Vanadium and chromium contents are between 3.2 and 13.3 ppm, and between 5.8 and 15.1 ppm, respectively. Al_2O_3 contents are from 720 to 1560 ppm and TiO_2 from 25 to 40 ppm.
- *type* (*e*) is a grey to white coarse-grained marble (N4 sample, Table 1) with low MgO contents (MgO ~ 3.6 wt%) but enriched in aluminium (up to 0.59 wt%). Titanium content is up to 1300 ppm, whereas chromium and vanadium are 24 and 11 ppm, respectively.

The grey carbonate-bearing bands are located in types (d) and (e) marbles. They are generally calcitic (MgO less than 4 wt%) in composition but one sample (LKT2c) has MgO contents up to 17.2 wt% (Table 1). Chromium and vanadium contents are between 3 and 15 ppm, whereas aluminium is between 1300 and 3200 ppm (Table 2).

The schist unit is 10–15 m thick and exposed on both flanks of the Nangimali syncline, enclosing the unit of ruby-bearing marbles. This level is a marker horizon for ruby mineralisation (Hamid, 1985). The contact with the underlying unit is gradual. Two types of rocks are distinguished by their mineralogy and geochemistry (Table 1): garnet-biotite schists and calc-schists. These metamorphic rocks clearly exhibit the same chemical composition as shales and marls bearing illite ± calcite ± dolomite from common platform series (Fig. 6), overlying the geochemical domain defined by Moine et al. (1981). Vanadium contents are between 71 and 239 ppm and chromium between 94 and 163 ppm (Table 2).

4.3. Carbon and oxygen isotopic signatures of Nangimali marbles

Stable isotope compositions are reported in Table 3. Carbonates from the Nangimali marbles vary in composition between calcite and dolomite end-members (Fig. 7(C)). They have $\delta^{13}C_{calcite}$ and $\delta^{18}O_{calcite}$ values that range from −1.9 to 2.4‰ and from 24.3 to 27.6‰, respectively. The $\delta^{13}C_{dolomite}$ and $\delta^{18}O_{dolomite}$ values are between −1.6 and 2.6‰ and 23.6 and 27.2‰, respectively. The $\delta^{13}C$ and the $\delta^{18}O$-values of the carbonates from the carbonate-bearing bands are between −1.59 and 1.75‰ and 25.0 and 25.9‰, respectively. These values are within the isotopic range defined for the marbles. Only one sample (N6) from yellowish marbles (type d) shows a clear shift towards lower $\delta^{18}O$ values ($\delta^{18}O = 22.00‰$) while the $\delta^{13}C$ fits in the range of the carbonates ($\delta^{13}C = 1.10‰$). In all other samples, the C–O isotopic compositions of calcite–dolomite pairs are close to high-temperature equilibrium values (Fig. 7(A) and (B)).

The isotopic compositions of graphite and calcite are given in Table 3. The two analysed samples have high $\delta^{13}C$ (graphite) values ranging from −3.2 to −2.7‰ and small Δ(calcite–graphite), ranging from 4.0 to 4.3. Values of Δ(calcite–graphite) decrease with increasing grade of metamorphism and the narrow equilibrated range found in

Table 1
Some typical chemical compositions of rocks from the Nangimali Formation (Lower and Upper members). Major element and trace element concentrations obtained by ICP-MS, respectively, in wt% and in ppm. Abbreviations: LK and MK = samples from Khora area; N = samples from Nangimali Top area; * = analysis obtained by wet chemistry (Al_2O_3 and TiO_2 elements)

Sample	Lower Member	Upper Member									
		Pyrite-bearing marble unit					Schists unit		Ruby-bearing marble unit		
	Amphibolite	Marbles					calc-schist	biotite schist	Marbles		Carbonate-bearing band
MKT3	LK2g (type a)	MKT1a (type b)	MKT2 (type b)	LKT2a′2 (type b)	LK1a (type c)	OO-P2	OO-P1	LK4 (type d)	N4 (type e)	LKT2C	
SiO_2	46.6	0.77	3.82	1.22	0.54	6.1	37.67	60.28	–	–	0.46
Al_2O_3	16.82	0.44	1.44	0.32	0.12	3.6	9.56	16.77	0.072*	0.59	0.32
Fe_2O_3	11.27	–	1.2	–	–	1.21	3.05	7.25	–	–	–
MnO	0.16	–	–	–	–	0.03	0.03	0.08	–	–	–
MgO	7.05	6.46	2.46	0.83	1.31	12.7	3.52	3.72	21.31	3.57	17.22
CaO	10.03	47.14	49.39	53.66	54.37	34.4	23.69	2.48	31.88	50.51	35.16
Na_2O	3.35	0.0193*	0.08	–	–	–	0.27	1.86	–	–	–
K_2O	1.0	0.08	0.32	0.13	0.0068*	0.81	3.55	4.86	–	–	0.08
TiO_2	1.25	0.0193*	0.08	0.0241*	0.0068*	0.18	0.45	0.81	0.0025*	0.13	0.0057*
P2O5	0.14	–	–	–	–	–	0.13	0.19	–	–	–
I.L.	2.17	43.93	39.29	42.81	43.45	38.87	17.91	1.55	44.86	43.55	44.76
Total	99.84	98.82	98.08	98.97	99.67	97.9	99.83	99.85	98.05	98.35	98.00
Ba	201	4.3	14.5	8.5	3.6	35	162	596	–	–	4.8
Cr	139	6.9	19.1	10.0	–	29.9	71	94	5.8	24	15
Sr	262	188	276	354	271	222	295	151	127	114	451
V	240	6	21.4	5.8	45	45	72	136	3.2	11	10.5

Table 2
Trace element concentrations (Cr, V, Al_2O_3 and TiO_2) in the ruby-bearing marbles from the Nangimali Formation (wet chemistry analysis). Abbreviations: LK and MK = samples from Khora area; N = samples from Nangimali Top area

Mine and sample	Ruby-bearing marbles unit (ppm)			
	Cr[a]	V[a]	Al_2O_3[b]	TiO_2[b]
Yellowish to white marble (type d)				
Khorat				
LK4	5.8	3.2	720	25
LKT4b	8	5.5	1000	30
LKT13	7.9	3.9	980	25
LKT1b1	14.9	4.7	1470	33
LKT10	15.1	13.3	1560	35
LKT3	8.9	4.5	1410	40
OO-P5a	10.8	6.9	1440	35
Nangimali				
N3[c]	23	12.6	3900	77
Grey marble (type e)				
Nangimali				
N4	24	10.8	5900	1300

[a] Cr and V analysed by ICP-MS.
[b] Al_2O_3 and TiO_2 analysed by wet chemistry.
[c] Sample located at the border of a shear-zone.

Nangimali is typical of upper amphibolite and granulite facies (Dunn and Valley, 1992). Due to the high sensitivity to temperature, carbon isotope thermometry is useful for determining the temperatures in moderate to high-grade metamorphosed carbonate rocks. The two calcite–graphite pairs give regional metamorphic temperatures of 630–645 °C in agreement with the amphibolite grade affecting the Nangimali Formation.

4.4. Geochronological data

The present study carried out using four samples of phlogopite selected from the Lower Khora ruby mine. Argon isotopic results for analysed minerals are given in Table 4.

Sample LK1a (Fig. 4(A)) is located in a pyrite–phlogopite-bearing marble (type c). Phlogopite is developed in the foliation of the metamorphic formation. The phlogopite yields a well-defined plateau age (Fig. 8(A)) of 16.1 ± 0.2 Ma for nearly 97% of the ^{39}Ar released (calculated on 11 steps).

Sample LK3 (Fig. 4(B)) corresponds to a phlogopite originating from a marble (type d) affected by a pervasive fluid-alteration along micro-fractures. It is characterised by the development of masses of phlogopite and pyrite parallel or slightly discordant to the metamorphic foliation. The marble contains phlogopite, pyrite, ± ruby, and calcite with dolomite. Mica flakes were picked out from fractures discordant to the foliation. Phlogopite displays an age plateau defined at 15.3 ± 0.1 Ma for nearly 94% of the ^{39}Ar degassed (Fig. 8(B)).

Sample LKT1d (Fig. 4(C)) is a phlogopite-bearing marble (type d) affected by folding. A second generation of phlogopite associated with pyrite and graphite is developed in the axial plane of the fold. The syn-deformational phlogopite yields an age of 17.2 ± 0.2 Ma obtained for more than 90% of released argon (Fig. 8(C)).

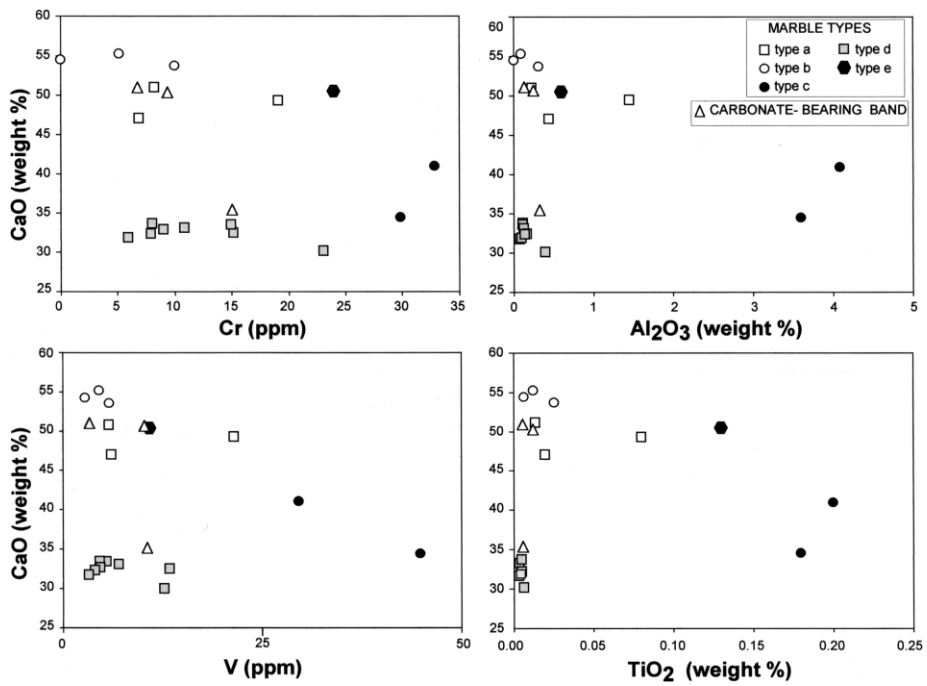

Fig. 5. CaO (wt%) versus Cr (ppm), V (ppm), Al_2O_3 (wt%) and TiO_2 (wt%) variations in Nangimali marbles and carbonate-bearing bands (Upper member of the Nangimali Formation).

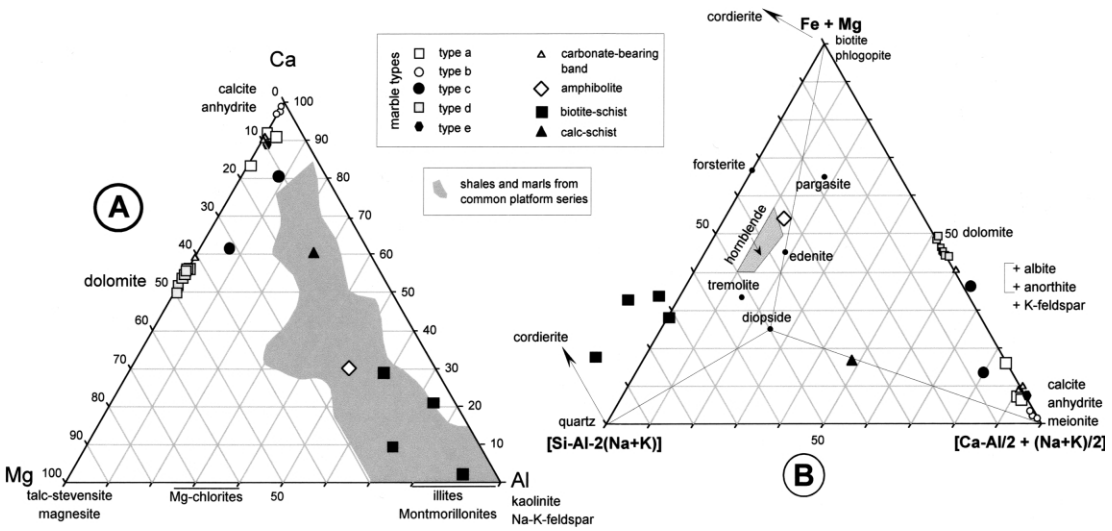

Fig. 6. (A) Al–Mg–Ca diagram (in milliatoms) showing the geochemical distribution of the schists and the marbles from the Nangimali Formation. The schists fit within the geochemical domain of shales and marls from the common platform series. Type c marbles exhibit higher Al contents due to the presence of phlogopite in the carbonate rocks. (B) Projection of the QCAF tetrahedron from anorthite on the QCF plane (Q = Si–3Na–3K; C = Ca; A = Al–Na–K; F = Fe + Mg, in milliatoms).

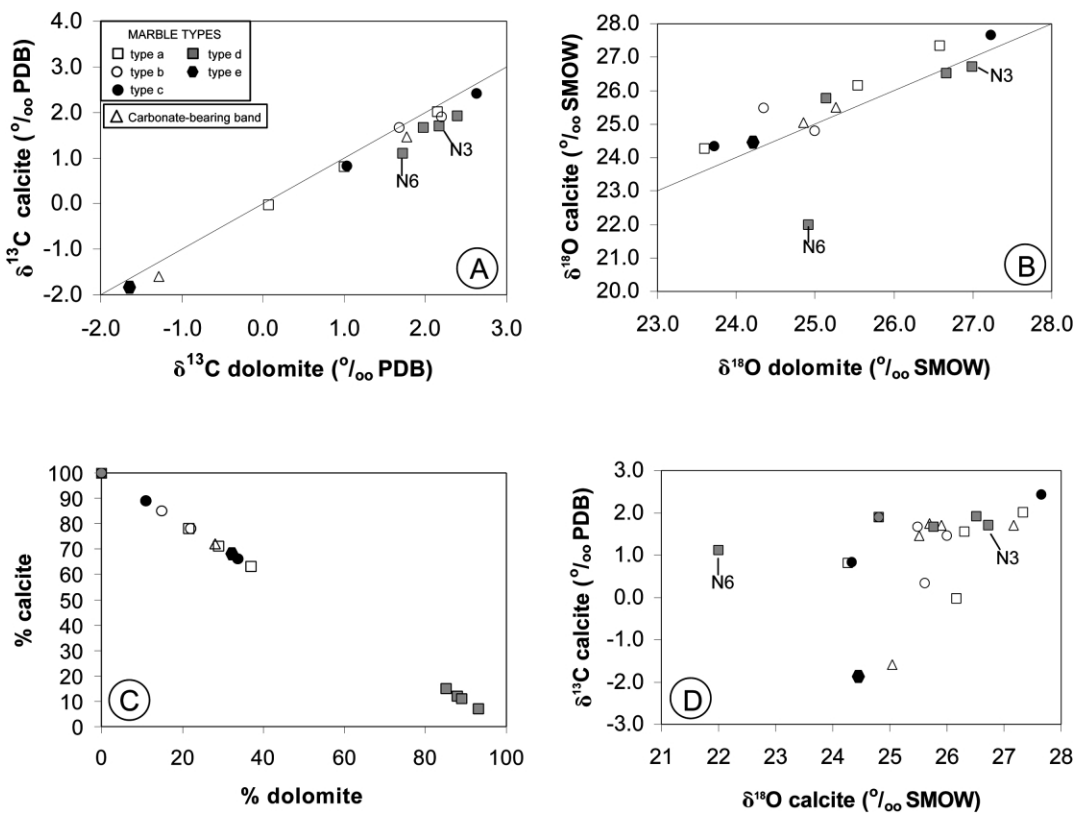

Fig. 7. Carbon and oxygen isotopic signatures of marbles from the Nangimali Formation. (A) and (B) Carbon and oxygen isotopic compositions of coexisting calcite and dolomite in the different types of marble. Except for sample N6, calcite and dolomite are fairly close to high temperature isotopic equilibrium (defined by the line of slope 1; Sheppard and Schwarcz, 1970). Sample N3 is a marble located at the border of a shear-zone. (C) Mixing ratios of CO_2 evolved from calcite and dolomite of the studied marbles (in % CO_2). (D) δ^{13}C calcite (‰, PDB) versus δ^{18}O calcite (‰, SMOW) diagram for the Nangimali marbles.

Table 3
Stable isotope compositions of Nangimali marbles (Upper member of the Nangimali Formation). All the $^{18}O/^{16}O$ and $^{13}C/^{12}C$ are reported relative to Standard Mean Ocean Water (SMOW) and Peedee belemnite (PDB), respectively

Sample	Calcite		Dolomite		Graphite $\delta^{13}C$ (‰ PDB)	ΔCal–Gr[a]	Temperature (calcite − graphite pair) (°C)
	$\delta^{13}C$ (‰ PDB)	$\delta^{18}O$ (‰ SMOW)	$\delta^{13}C$ (‰ PDB)	$\delta^{18}O$ (‰ SMOW)			
Pyrite-bearing marbles							
Marble type a							
LKT2a′	0.81	24.27	1.00	23.60	−3.22	4.03	647 ± 23[b]
LKT2f′2	−0.03	26.16	0.07	25.54			
LKT2i′	2.01	27.34	2.15	26.58			
LK2g	1.55	26.30					
Marble type b							
MKT2	1.67	25.49	1.68	24.35	−2.68	4.35	631 ± 11[c]
LKT1bb	1.90	24.80	2.20	25.00			
LKT2b	1.45	26.00					
LKT2f′1	0.33	25.61					
Marble type c							
LKT2g′	2.42	27.65	2.64	27.23			
LKT2c′	0.83	24.33	1.03	23.72			
Ruby-bearing marbles							
Marble type d							
N3[d]	1.70	26.73	2.17	26.99			
N6	1.11	22.00	1.72	24.92			
LKT13	1.66	25.76	1.98	25.14			
LK4	1.92	26.51	2.40	26.66			
Marble type e							
N4	−1.87	24.45	−1.64	24.20			
Carbonate-bearing band							
N1	−1.59	25.04	−1.29	24.85			
LKT2h′	1.7	27.17					
LKT4-a	1.46	25.51	1.77	25.26			
LKT1Cg	1.70	25.90					
MKT1a	1.75	25.70					

[a] $\Delta_{Cal\_Gr} = \delta^{13}C_{calcite} - \delta^{13}C_{graphite}$.
[b] Mean of the temperatures obtained with the geothermometers of Valley and O'Neil (1981), Kreulen and Van Beek (1983), Wada and Suzuki (1983), Dunn and Valley (1992) and Kitchen and Valley (1995).
[c] Mean of the temperatures obtained with the geothermometers of Kreulen and Van Beek (1983), Dunn and Valley (1992) and Wada and Suzuki (1998).
[d] Sample located at the border of a shear-zone.

Sample LKT10 (Fig. 4(D)) is a phlogopite originating from a pyrite–phlogopite–ruby-bearing gash vein linked to a small-scale shear-zone. Phlogopite is coeval with the deposition of ruby and displays an age plateau defined at 16.1 ± 0.5 Ma (Fig. 8(D)) for more than 90% of the ^{39}Ar released (calculated on 9 steps).

5. Discussion

5.1. Source of aluminium in ruby

The marbles of the upper member of the Nangimali Formation vary in composition from Ca-rich to Mg-rich. Grey and white marbles (types a, b, e) are calcite-rich and yellowish marbles (type d) are dolomite-rich. The mineralogy is simple and composed by the end-member calcite or dolomite ± (pyrite, phlogopite). Graphite and dravite have been found only in the marbles of types (a) and (b) but neither garnet, spinel, forsterite nor pyroxene were observed. Marbles of type (c) are impure and contain variable amounts of phlogopite and pyrite (Fig. 4(A)). The carbonate-bearing bands intercalated in marbles of types (d) and (e) are calcite or dolomite-rich.

The ore-bearing zone, 6 and 3 m thick, respectively, in the Nangimali and Khora areas, contain ruby either in discontinuous and millimetre to centimetre thick veinlets and gash veins or disseminated crystals around the veins and

Table 4
Argon isotopic results for analysed phlogopites. Reported errors are 1 sigma (1σ) for plateau and total ages, which include uncertainties of the monitors and their $^{40}Ar/^{39}Ar$ ratios. Correction interference used for $^{36}Ar/^{37}Ar_{Ca}$ is 2.93×10^{-4}. Mass discrimination factor is calculated for $^{40}Ar/^{36}Ar$ ratio of 291

Steps	$^{40}Ar^{*}/^{39}Ar$	$^{36}Ar/^{40}Ar$	$^{39}Ar/^{40}Ar$	$^{37}Ar/^{39}Ar$	% Atm	% ^{39}Ar	Age ± 1S.D.
LK1a phlogopite (J = 0.014273)							
1	0.497	1.864	0.902	0.000	55.1	1.4	12.8 ± 2.5
2	0.527	2.068	0.736	0.000	61.1	4.8	13.5 ± 0.9
3	0.581	1.400	1.007	0.000	41.4	7.7	14.9 ± 1.3
4	0.620	0.839	1.211	0.063	24.7	8.6	15.9 ± 0.5
5	0.614	0.507	1.383	0.244	15.0	10.1	15.7 ± 0.0
6	0.627	0.422	1.393	0.004	12.5	13.4	16.1 ± 0.2
7	0.639	0.191	1.476	0.000	5.7	18.6	16.4 ± 0.7
8	0.631	0.220	1.481	0.016	6.5	42.6	16.2 ± 0.1
9	0.625	0.449	1.385	0.033	13.3	63.0	16.0 ± 0.2
10	0.619	0.319	1.461	0.041	9.4	73.9	15.9 ± 0.4
11	0.661	0.000	1.511	0.000	0.01	86.3	16.9 ± 0.3
12	0.620	0.224	1.505	0.000	6.6	99.0	15.9 ± 0.3
13	0.582	0.421	1.503	0.057	12.5	100	14.9 ± 2.7
							Total age = 15.9 ± 0.2 Ma
LK3 phlogopite (J = 0.014273)							
1	2.719	2.712	0.073	0.070	80.1	0.0	68.7 ± 50.4
2	1.160	2.383	0.254	0.857	70.4	0.2	29.6 ± 1100
3	0.315	2.629	0.707	0.230	77.7	0.9	8.11 ± 3.7
4	0.207	2.899	0.691	0.721	85.6	1.9	5.3 ± 300
5	0.244	2.485	1.085	0.044	73.4	2.7	6.3 ± 4.4
6	0.462	1.081	1.470	0.015	31.9	5.4	11.9 ± 100
7	0.551	0.608	1.486	0.000	17.9	10.0	14.1 ± 0.6
8	0.563	0.459	1.532	0.000	13.5	22.8	14.5 ± 0.2
9	0.604	0.148	1.580	0.000	4.3	99.8	15.5 ± 0.1
							Total age = 15.0 ± 0.2 Ma
LKT1d phlogopite (J = 0.014273)							
1	2.368	2.252	0.141	0.000	66.5	0.1	60.0 ± 17.8
2	1.440	3.306	0.015	0.000	97.7	0.4	36.7 ± 31.8
3	1.553	0.300	0.586	0.000	8.8	0.7	39.6 ± 16.3
4	0.970	0.762	0.798	0.000	22.5	1.9	24.8 ± 25.7
5	0.705	2.253	0.473	0.000	66.6	2.9	18.1 ± 4.8
6	0.716	2.421	0.397	0.016	71.5	5.3	18.3 ± 2.5
7	0.673	0.752	1.154	0.002	22.2	100	17.3 ± 0.1
							Total age = 17.5 ± 0.4 Ma
LKT10 phlogopite (J = 0.02251)							
1	0.183	2.624	1.226	0.059	77.5	0.3	7.4 ± 9.9
2	0.347	1.904	1.257	0.106	56.2	0.9	14.1 ± 4.9
3	0.301	2.501	0.866	0.053	73.9	1.6	12.2 ± 6.1
4	0.002	3.375	1.159	0.116	99.7	2.1	0.1 ± 7.4
5	0.407	1.515	1.174	0.069	44.7	2.7	19.0 ± 2.2
6	0.354	2.284	0.917	0.011	67.5	3.5	14.3 ± 2.7
7	0.377	0.94	1.913	0.000	27.7	5.0	15.3 ± 2.5
8	0.441	0.846	1.7	0.000	25.0	5.6	17.8 ± 2.7
9	0.421	0.251	2.194	0.000	7.4	8.0	17.1 ± 0.7
10	0.364	0.505	2.332	0.000	14.9	10.9	14.8 ± 0.7
11	0.383	0.232	2.428	0.000	6.8	16.2	15.5 ± 0.5
12	0.407	0.000	2.456	0.000	0.0	28.0	16.5 ± 0.1
13	0.392	0.132	2.448	0.000	3.9	89.7	15.9 ± 0.1
14	0.419	1.076	1.624	0.000	31.8	96.6	17.0 ± 0.3
15	0.406	0.015	2.449	0.000	0.4	98.5	16.4 ± 0.1
16	0.428	0.217	2.184	0.000	6.4	100	17.3 ± 0.2
							Total age = 16.0 ± 0.1 Ma

in the carbonate-bearing bands. Pargasite and margarite are restricted to the ore-bearing zone within the grey and yellowish marbles or in the carbonate-bearing bands. The presence of Na-amphibole in the ore-zone implies either that the marbles or the carbonate bands were originally Na-bearing or that sodium was introduced by the mineralising fluids. The preliminary fluid-inclusion study in ruby showed only the presence of carbonic fluids (Giuliani

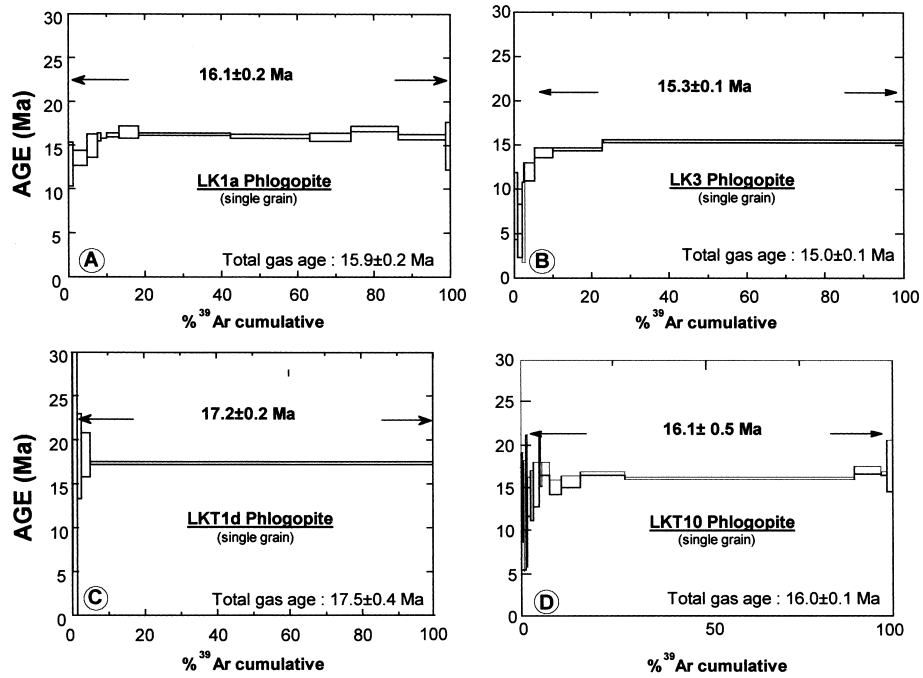

Fig. 8. $^{40}Ar/^{39}Ar$ age spectra of phlogopites from the ruby-bearing marbles of the Lower Khora mine in the Nangimali Formation.

et al., in preparation) and the ruby-bearing marbles do not contain sodium. The original nature of the carbonate bands are unknown but a sodium-bearing mineralogy remains possible (evaporitic lenses ?).

The source of the chemical elements composing ruby is always in debate for ruby hosted in marbles (Giuliani et al., 2000). Aluminium, chromium, vanadium, iron and titanium may be present in the host rock or carried by an external fluid infiltrating the series. These elements may originate from two main sources:

(i) The schists. A shear-system developed in the inner part of the Nangimali syncline and one can imagine that the garnet-biotite schists, exposed on both flanks of the isoclinal fold, were also sheared and leached by the incoming fluid. The quantity of Al–Cr–V–Fe–Ti in the schists is sufficient to form ruby (Table 1). Nevertheless, there is no evidence in the field of shearing in these rocks.

(ii) The yellowish and grey marbles (types d and e). Table 2 shows significant contents of aluminium between 720 and 5900 ppm in both types. The concentrations in Cr, V, Fe, and Ti (Fig. 5) are also sufficient to be incorporated in the ruby. The titanium contents between 25 and 1300 ppm may also explain the deposition of rutile, which is a main phase coeval with ruby.

The resource potential of the ore area was estimated for the Khora and Nangimali Top (Malik, 1994). In Khora, the estimated volume calculated on a 200 m strike length, 160 m dip length and a thickness of 3 m, is 96,000 m^3. The grade of 11 g/m^3 based on 3 years pilot scale permitted to estimate a ruby potential of 1056 kg. In Nangimali Top, the ore potential has been estimated to be 1260 kg (area triangle 160 m × 240 m, thickness = 6 m, volume of 1,15,200 m^3, average grade 11 g/m^3). Mass-balance calculation of the potential of ruby, based on the amount of Al_2O_3 potentially mobile from the host marbles (1000 ppm in the yellow marble), the density of 2.8 g/cm^3 of the marble and the respective volumes of the ore-zones, leads to $\sim 2688 \times 10^2$ and 1930×10^3 kg of Al_2O_3 available for Khora and Nangimali Top, respectively. The ruby resource potential estimated by Malik (1994) corresponds for both zones to ~0.4% of these maximum ruby reserves when considering the totality of Al_2O_3 mobilised by the fluids. In fact, the whole marbles in the ore-zone are not affected by a pervasive alteration and the quantity of leached aluminium may originate from the volume of marble affected by the small-scale shear-zones. A calculation based on a reserve of 1056 kg of ruby in Khora and on the 1000 ppm contained in the yellowish marble, leads to determine a leached marble block of 200 m strike length, 160 m dip length and 0.8 cm thick. These mass-balance calculations are realistic considering the geometry of the veinlets (generally less than 1 cm thick) and show that the amount of Al_2O_3 contained in the marbles is sufficient to supply the hydrothermal system in aluminium for deposition of ruby.

5.2. Origin of the mineralising fluids

The oxygen and carbon isotopic values from the marbles span the range defined for most of marine carbonates ($\delta^{13}C = 0 \pm 40‰$), regardless of the age of formation

(Ohmoto and Rye, 1979). The metamorphism has induced no fractionation between carbonates of the marbles and the metamorphosed protholith as shown in the $\delta^{13}C$ verus $\delta^{18}O$ diagram (Fig. 7(D)) where no variations nor trends are defined. Sample N6 is enriched by 2‰ in ^{18}O relatively to the mean $\delta^{18}O$-value of the marbles. Two hypothesis may explain the ^{18}O-shift: (i) metamorphic devolatilisation reactions in carbonate rocks release a mixed CO_2-H_2O fluid enriched in ^{18}O and ^{13}C with respect to the isotopic composition of the bulk rock. Loss of this fluid during decarbonation may lower the $\delta^{18}O$-values (Valley, 1986); (ii) combined fluid infiltration and devolatilisation during metamorphism will also lowered the $\delta^{18}O$ and $\delta^{13}C$-values (Valley, 1986). Nevertheless, hypothesis (ii) will induce a large scale lowering of $\delta^{18}O$ values ($>3-4$‰) and will introduce a positive correlation between $\delta^{13}C$ and $\delta^{18}O$. Besides, the $\delta^{13}C$ of the carbonates show relatively little scatter and are consistent with metamorphic decarbonation. Therefore, the range of isotope data is best explained by Rayleigh decarbonation during metamorphism without fluid flow (hypothesis i).

Fluid infiltration in the marbles is limited to the ruby-bearing small-scale shear-zones. Sample N3 corresponds to a yellowish marble occurring at the border of a shear-zone; its C- and O-isotopic signatures are within the isotopic domain defined by the whole marbles. Therefore, we conclude that limited fluid infiltration had no effect on the $\delta^{18}O$ and $\delta^{13}C$-values of carbonates, because the C–O composition of the infiltrating fluids was not greatly out of isotopic equilibrium with the marble. Pervasive syn-metamorphic infiltration may have involved fluids marked by different origins: (i) crustal fluids in equilibrium with syn-metamorphic granitic intrusions like the Chichi granite located at the North of Shonthar Gali (range of $\delta^{18}O$-values for granites between 10 and 13‰, Sheppard, 1986), (ii) carbonic fluids derived from the mantle ($\delta^{18}O \sim 12$‰, Pineau and Javoy, 1994) and (iii) crustal fluids in equilibrium with metamorphism ($\delta^{18}O \sim 22-25$‰). The mixing of fluids (i) or (ii), characterised by contrasting isotopic signatures with decarbonation metamorphic fluids (iii) might provoke extensive oxygen isotopic alteration and also a decrease in $\delta^{18}O$ and $\delta^{13}C$, before reaching the value of a fluid-buffering system (Valley, 1986). The observed cluster of data is totally in disagreement with such hypothesis and the Nangimali fluid appears to be metamorphic in origin (fluid iii).

5.3. Formation age of ruby and cooling history of the Nanga Parbat massif

The $^{40}Ar/^{39}Ar$ data obtained on phlogopites from the Nangimali ruby deposit are not significantly different in age. The four micas record ages of 15.3, 16.1, 17.2 and 16.1 Ma, respectively, characterising a single thermal event in the Nangimali area. For each sample, the age spectrum does not suggest argon loss by diffusion processes or excess argon incorporated in the phlogopite crystals during their development. Phlogopites LKT1d and LK3 record ages of 17.2 ± 0.2 and 15.3 ± 0.1 Ma, respectively, corresponding to the last increments of experimental degassing. The age plateaus were calculated only on the three steps, which represented more than 90% of the ^{39}Ar released. This range of ages includes the well-defined plateau ages defined for phlogopite LK1a at 16.1 ± 0.2 Ma and for phlogopite LKT10 at 16.1 ± 0.5 Ma.

Calcite–graphite isotopic geothermometry in marbles from the Nangimali deposit indicates temperatures of 630–645 °C, higher than the closure temperature of dated phlogopites (415 ± 40 °C; Giletti, 1974). Therefore, we consider the age range 15.3–17.2 Ma, to be a record of Neogene cooling of the Nangimali area. Besides, the age range helps to establish the minimum formation age of ruby at 16 Ma. The Nangimali ruby deposit crossed the 375–450 °C isotherms during Lower Miocene time (Langhian–Burdigalian stages). In the Chichi valley, north of the Shontar Gali area, the Ar–Ar cooling age of the Chichi granite is determined to be 19 Ma (Schneider et al., 1999c). This age is very close to the cooling ages found for the Nangimali ruby mineralisation and one could imagine a direct link between granite emplacement and ruby formation in the area. However, we note that the isotopic trends of both $\delta^{18}O$ and $\delta^{13}C$-values for the carbonate rocks and the infiltrated marbles discussed earlier are inconsistent with such a scenario.

Numerous ages are now available across the Himalayan western syntaxis, mainly in the Nanga Parbat Himalayan gneisses spur. Ages obtained by Zeitler et al. (1989, 1993), Schneider et al. (1999a,b) and also Treloar et al. (2000a,b) show the complexity of the evolution of the zone in which Precambrian magmatism and metamorphism have been largely obliterated by the Himalayan thermal evolution, most probably in the last 45 Ma (Smith et al., 1994). Nevertheless, attention has been concentrated on the cooling ages, which document a spectacular late Miocene–Neogene thermal evolution in the central and northern Nanga Parbat massif. East of the Raikhot fault, the northernmost part of the massif corresponds to the western extremity of an EW trending elongated zone of structural domes, first recognised in the Southern Karakorum (Lemennicier et al., 1996; Pêcher and Le Fort, 1999; Rolland et al., 2002). In this region, the high temperature granulite-facies metamorphism imprint is dated between 5 and 10 Ma. Further south, in the Nanga Parbat summit area, cooling ages as young as 1 Ma are found (Zeitler et al., 1993). This thermal evolution ends with emplacement of late leucogranites whose ages also decrease southward across the massif: in the North East, the Jutial pluton crystallised at 10 Ma (Schneider et al., 1999b), while in the central portion of the massif, the Tato and Mazeno Pass plutons crystallised at 1 and 1.4 Ma respectively (Zeitler et al., 1993; Schneider et al., 1999b).

In a similar way, thermochronology of the SW region of the Nanga Parbat–Haramosh massif has shown that cooling

ages of the rocks increased west across the massif into the Indian cover metasediments (Edwards et al., 2000). Cooling ages between 1 and 5 Ma found east of the Diamir shear-zone, mechanically linked to part of the Raikhot fault system, present ages typical of Nanga Parbat rocks (Schneider et al., 1997). To the west of the Diamir shear-zone, older cooling ages, up to 40 Ma, are found in the Babusar area (Chamberlain et al., 1991) and in the Hazara syntaxis (Smith et al., 1994).

Finally, in the NE region of the massif at the Karakorum–Nanga Parbat–Haramosh junction, diachronous metamorphism was evidenced at 35–40 Ma in the Indus valley, which was followed by a contrasting exhumation styles at 10–15 Ma (Villa et al., 1996).

Our Early Miocene ages, found in rocks located in the southern part of the Nanga Parbat spur, at 30 km south-east of the Diamir shear-zone, do not result from excess radiogenic argon as found for some of the rocks of the Indian cover (Chamberlain et al., 1991), but emphasise a lower Miocene thermal event. They compare to those found in the Zangot and Pharlobat-Rollo regions of the Diamir shear-zone, with ages between 10 and 20 Ma (Edwards et al., 2000) and also with cooling age profiles performed across the Raikhot Liachar fault system in the northern part of the Nanga Parbat–Haramosh massif (Zeitler, 1985; George et al., 1995). Combined with previous data (mainly Treloar et al., 2000a,b; Schneider et al., 2001), our results allow the drawing of a rather complete cooling age map of the Nanga Parbat area (Fig. 1, argon ages). It clearly shows the extrusion of the central deep-crustal pop-up corner of the massif, controlled by the main Diamir and Rupal shear-zones. Their southern continuation are the Gumot shear-zone (Malik et al., 1996), which is the direct prolongation of the Diamir shear-zone, and the highly stretched orthogneisses in the Bunda Nar valley, west of Nangimali, which probably trace the Rupal shear-zone.

Our new Ar–Ar data date rocks located south and outside the Nanga Parbat spur, and are similar to ages obtained in the neighbouring Chichi granite, only 10 km to the north. Thus, in the southern part of the Nanga Parbat transverse crustal fold, the Early to Middle Miocene metamorphism and anatexis, ubiquitous elsewhere in the Central Himalaya, could also be the dominant thermal event. However, it is linked to north-vergent folds, a feature which questions the modalities of the Himalayan piling in this area, and the importance of southward tilting of the whole pile, probably related to vertical extrusion of the Nanga Parbat massif.

6. Conclusions

The Nangimali ruby deposit represents an interesting case study of ruby formation by fluid transfer during metamorphic processes. Ruby genesis does not record a contribution of a mantle or crustal-derived carbon source originating from granitoids. Decarbonation fluids coupled with fluid/rock interaction related to shearing and channelled fluid circulation appear to be a satisfactory mechanism for ruby genesis.

The marbles form a potential proximal source for aluminium but also for chromium and vanadium incorporated into the ruby structure. Mass-balance calculations based on the ore grade and the total volume of ruby extracted during a 3 years period, coupled with the fact that marbles contain 1000 ppm Al_2O_3, suggest that mobilisation of aluminium in the shear-zone is sufficient to account for all ruby production in the mine.

Dating of phlogopite crystals syngenetic or coeval with ruby defines a cooling age at 16 Ma, thus suggesting a minimum Miocene age for ruby formation. From a regional point of view, these new Neogene cooling ages compliment the numerous data available elsewhere in this poorly documented region of the Nanga Parbat–Haramosh spur. They are consistent with ages between 10 and 20 Ma found in the western and eastern borders of the Nanga Parbat massif. A cooling age map can therefore be drawn around the whole Nanga Parbat, which clearly outlines the extrusion of the central deep-crustal pop-up corner of the massif.

Acknowledgements

This study was supported by the co-operative program DSUR-PAK-4C5-013 entitled ‘Echanges et Recherches dans le Domaine de la Géologie de Haute Montagne’ between the University J. Fourier (Laboratoire de Géodynamique des Chaînes Alpines, Grenoble), CRPG/CNRS (Centre de Recherches Pétrographiques et Géochimiques, Vandœuvre), IRD (Institut de Recherche pour le Développement, Paris) and the Geological Survey of Pakistan (Islamabad). The authors wish to thank Azad Kashmir Mineral and Industrial Development Corporation, Muzaffarabad (Azad Kashmir, Pakistan) for logistic assistance during field work. Thanks to the geologists Naseem, Kiane, Shoukat, Shohab and Zameer for their help during the field work. We are grateful to Dr Alain Dhersigny, Counsellor for Cultural, Scientific and Technical Co-operation in the French Embassy in Pakistan, who supported financially and scientifically the project. Thanks also go to N. Arndt, W.L. Brown and M. Topliss for English corrections. We are grateful to R. Rolfo, C.A. Hauzenberger and K. Stüwe for their reviews that greatly improved the clarity and quality of this paper.

References

Argles, T.W., 2000. The evolution of the Main Mantle Thrust in the Western Syntaxis, Northern Pakistan. Geological Society, Special Publication, London 170, 101–122.

Butler, R.W.H., Prior, D.J., Knipe, R.J., 1989. Neotectonics of the Nanga Parbat syntaxis, Pakistan, and crustal stacking in the Northwest Himalaya. Earth and Planetary Science Letters 94, 329–343.

Butler, R., George, M., Harris, N., Jones, C., Prior, D., Treloar, P., Wheeler, J., 1992. Geology of the northern part of the Nanga Parbat massif, northern Pakistan, and its implications for Himalayan tectonics. Journal of the Geological Society of London 149, 557–567.

Butler, R.W.H., Wheeler, J., Treloar, P.J., Jones, C., 2000. Geological structure of the Southern part of Nanga Parbat massif, Pakistan Himalaya, and its tectonic implications. Geological Society, Special Publication, London 170, 123–136.

Chamberlain, C.P., Zeitler, P.K., Erickson, E., 1991. Constraints on the tectonic evolution of the north-western Himalaya from geochronologic and petrologic studies of Babusar Pass, Pakistan. Journal of Geology 99, 829–849.

Chamberlain, C.P., Zeitler, P.K., 1996. Assembly of the crystalline terranes of northwestern Himalaya and Karakoram, northwestern Pakistan. In: An, Y., Harrison, M.T. (Eds.), The Tectonic Evolution of Asia, Cambridge University Press, New York, pp. 138–149.

Chaudry, M.N., Ghazanfar, M., 1987. Geology, structure and geomorphology of upper Kaghan valley, Northwestern Himalaya, Pakistan. Geological Bulletin University of Punjab 22, 13–57.

Coward, M.P., Windley, B.F., Broughton, R.D., Luff, I.W., Petterson, M.G., Pudsey, C.J., Rex, D.C., Khan, A., 1986. Collision tectonics in the north-west Himalayas. In: Coward, M.P., Ries, A.C. (Eds.), Collision Tectonics, pp. 203–219.

DiPietro, J.A., Hussain, A., Ahmad, I., Khan, M.A., 2000. The Main Mantle Thrust in Pakistan: its character and extent. Geological Society, Special Publication, London 170, 375–393.

Dunn, S.R., Valley, J.W., 1992. Calcite–graphite isotope thermometry: a test for polymetamorphism in marble, Tudor gabbro aureole, Ontario, Canada. Journal of Metamorphic Geology 10, 487–501.

Edwards, M.A., Kidd, W.S.F., Khan, M.A., Schneider, D.A., Zeitler, P.K., 1997. Structural geology of the southwestern margin of Nanga Parbat. EOS Transactions, American Geophysical Union 236, F651.

Edwards, M.A., Kidd, W.S.F., Khan, M.A., Schneider, D.A., 2000. Tectonics of the SW margin of the Nanga Parbat–Haramosh massif. Geological Society, Special Publication, London 170, 77–100.

George, M.T., Reddy, S., Harris, N., 1995. Isotopic constraints on the cooling history of the Nanga Parbat–Haramosh massif and Kohistan arc, western Himalaya. Tectonics 14, 237–252.

Giletti, B.J., 1974. Studies in diffusion. I. Argon in phlogopite mica. In: Hofmann, A.W., et al. (Eds.), Geochemical Transport and Kinetics, Carnegie Institute of Washington, Washington, DC, pp. 107–115.

Giuliani, G., Garnier, V., Ohnenstetter, D., Schwarz, D., France-Lanord, Ch., Dubessy, J., Maluski, H., Kausar, A.B., Khan, T., Malik, R.H., Phan Trong, T., Hoáng Quang, V., 2000. Marble-hosted ruby deposits in south-east Asia: a review. In: Leroy, J., (Ed.), Metallogeny 2000, Nancy, pp. 67–68.

Greco, A., Martinotti, G., Papritz, K., Ramsay, J.G., Rey, R., 1989. The crystalline rocks of the Kaghan valley (NE Pakistan). Eclogae Geologicae Helvetiae 82, 629–653.

Hamid, K.A., 1985. Geological aspects of ruby occurrences of Khora and Nangimali Top: Muzaffarabad (AK), Pakistan, AKMDC, Unpublished report.

Hashmi, et al., 1990. Geology and mineral occurrences of Shontar valley: Muzzaffarabad (AJK), Pakistan. In: Malik, R.H. (Ed.), unpublished report, AKMIDC.

Honegger, K., 1983. Strukturen und Metamorphose im Zanskar Kristallin (Ladakh-Kashmir, Indien). Unpublished PhD Thesis, ETH Zurich.

Honegger, K., Dietrich, V., Frank, W., Gansser, A., Thöni, M., Trommsdorff, V., 1982. Magmatism and metamorphism in the Ladakh Himalayas (the Indus-Tsangpo suture zone). Earth and Planetary Science Letters 60, 253–292.

Khan, M.A., Jan, M.Q., Qazi, M.S., Khan, M.A., Shah, Y., Sajjad, A., 1995. Geology of the drainage divide between Kohistan and Kaghan, North Pakistan. Geological Bulletin University of Peshawar 28, 35–77.

Kreulen, R., Van Beek, P.C.J.M., 1983. The calcite-graphic isotope thermometer: data on graphite-bearing marbmes from Naxos, Greece. Geochim. Cosmochim. Acta, 47, 1527–1530.

Le Fort, P., Debon, F., Senet, J., 1980. The "Lesser Himalayan" Cordierite granite belt: typology and age of the pluton of Manserah Pakistan. Geol. Bull. Univ. Pehawar 13, p.51–61.

Lemennicier, Y., Le Fort, P., Lombardo, B., Pêcher, A., Rolfo, F., 1996. Tectonometamorphic evolution of the central Karakorum (Baltistan, northern Pakistan). Tectonophysics 260, 119–143.

Lombardo, B., Rolfo, F., Compagnoni, R., 2000. Glaucophane and barroisite eclogites from the Upper Kaghan nappe: implications for the metamorphic history of the NW Himalaya. Geological Society, Special Publication, London 170, 411–430.

Lombardo, B., Rolfo, F., 2000. Two contrasting eclogite types in Himalayas: implications for the Himalayan orogeny. Journal of Geodynamics 30, 37–60.

Malik, R.H., 1994. Geology and resource potential of Kashmir ruby deposits: Distt. Muzaffarabad (AK), Pakistan. Unpublished Report AKMIDC, p. 21.

Malik, R.H., Schouppe, M., Fontan, D., Verkaeren, J., Martinotti, G., Shaukat Ahmed, K., Quresh, S., 1996. Geology of the Neelum valley, district Muzaffarabad, Azad Kashmir, Pakistan. Geological Bulletin University of Peshawar 29, 91–111.

Madin, I.P., 1986. Structure and neotectonics of north-western Nanga Parbat–Haramosh Massif. MS Thesis, Oregon State University.

Madin, I.P., Lawrence, R.D., Ur-Rehman, S., 1989. The northwest Nanga Parbat–Haramosh massif: evidence for crustal uplift at the north-western corner of the Indian craton. Geological Society of America, Special Paper, London 232, 169–182.

McCrea, J.M., 1950. On the isotope chemistry of carbonates and a paleotemperature scale. Journal of Chemical Physics 18, 849–857.

McDougall, I., Harrison, T.M., 1988. Geochronology and thermochronology by the $^{40}Ar/^{39}Ar$ method., Clarendon Press, Oxford.

Mish, P., 1949. Metasomatic granitisation of batholitic dimensions. American Journal of Science 247, 209–249.

Moine, B., Sauvan, P., Jarousse, J., 1981. Geochemistry of evaporite-bearing series: a tentative guide for the identification of metaevaporites. Contribution to Mineralogy and Petrology 76, 401–412.

O'Brien, P.J., Zotov, N., Law, R., Khan, M.A., Jan, M.Q., 2001. Oesite in Himalayan eclogite and implications for models of India–Asia collision. Geology 29/5, 435–438.

Ohmoto, H., Rye, R.O., 1979. Isotopes of sulfur and carbon. In: Barnes, H.L., (Ed.), Geochemistry of Hydrothermal Ore Deposits, Second ed, Wiley, New York, pp. 509–567.

Papritz, K., Rey, R., 1989. Evidences for the occurrence of Permian Panjal Trap Basalts in the Lesser and Higher-Himalayas of Western Syntaxis Area, NE Pakistan. Eclogae Geologicae Helveticae 82, 603–627.

Pêcher, A., Le Fort, P., 1999. Late Miocene tectonic evolution of the Karakorum–Nanga Parbat contact zone (northern Pakistan). Geological Society of America, Special Paper 328, 145–158.

Pineau, F., Javoy, M., 1994. Strong degassing at ridge crests: the behaviour of dissolved carbon and water in basalt glasses at 14°N, Mid-Atlantic Ridge. Earth and Planetary Science Letters 123, 179–198.

Pognante, U., Spencer, D.A., 1991. First report of eclogites from the Himalayan belt, Kaghan valley, Northern Pakistan. European Journal of Mineralogy 3, 613–618.

Pognante, U., 1992. Different P-T-t paths and leucogranite occurences along the High Himalayan Crystalline: implications for subduction and collision along the Northern Indian margin. Geodinamica Acta 6, 5–17.

Rolland, Y., Mahéo, G., Guillot, S., Pêcher, A., 2002. Tectono-metamorphic evolution of the Karakoram Metamorphic Complex (Dassu-Askole area, NE Pakistan): mid-crustal granulite exhumation in a compressive context. Journal of Metamorphic Geology 19, 717–737.

Schneider, D.A., Zeitler, P.K., Edwards, M.A., Kidd, W.S.F., 1997. Geochronological constraints on the geometry and timing of anatexis and exhumation at Nanga Parbat: a progress report. EOS Transactions

of American Geophysical Union 78, Spring Meeting Supplement 17, 111.

Schneider, D.A., Edwards, M.A., Zeitler, P.K., Coath, C., 1998. Synkinematic magmatism within SW Nanga Parbat, Pakistan Himalaya. Geological Society of America Abstracts with Programs 30/7, A357.

Schneider, D.A., Edwards, M.A., Kidd, W.S.F., Asif Khan, M., Seeber, L., Zeitler, P.K., 1999a. Tectonics of Nanga Parbat, western Himalaya: Synkinematic plutonism within the doubly vergent shear-zones of crustal-scale pop-up structure. Geology 27, 999–1002.

Schneider, D.A., Edwards, M.A., Zeitler, P.K., Coath, C.D., 1999b. Mazeno Pass pluton and Jutial pluton, Pakistan Himalaya: age and implications for entrapment mechanisms of two granites in Himalaya. Contribution to Mineralogy and Petrology 136, 273–284.

Schneider, D.A., Edwards, M.A., Kidd, W.S.F., Zeitler, P.K., Coath, C.D., 1999c. Early Miocene anatexis identified in the western syntaxis, Pakistan Himalaya. Earth and Planetary Science Letters 167, 121–129.

Schneider, D.A., Zeitler, P.K., Kidd, W.S.F., Edwards, M.A., 2001. Geochronological constraints on the tectonic evolution and exhumation of Nanga Parbat, western Himalaya syntaxis, revisited. Journal of Geology 109, 563–584.

Seeber, L., Pêcher, A., 1998. Strain partitioning along the Himalayan arc and the Nanga Parbat antiform. Geology 26, 791–794.

Sheppard, S.M.F., 1986. Characterization and isotopic variations in natural waters. Mineralogical Society of America, Reviews in Mineralogy 16, 165–183.

Sheppard, S.M.F., Schwarcz, H.P., 1970. Fractionation of carbon and oxygen isotopes and magnesium between coexisting metamorphic calcite and dolomite. Contribution to Mineralogy and Petrology 26, 161–198.

Smith, H.A., Chamberlain, C.P., Zeitler, P., 1992. Documentation of the Neogene regional metamorphism in the Himalayas of Pakistan using U–Pb in monazite. Earth and Planetary Science Letters 113, 93–105.

Smith, H.A., Chamberlain, C.P., Zeitler, P.K., 1994. Timing and denudation of Himalayan metamorphism with the Indian Plate, NW Himalaya, Pakistan. Journal of Geology 103, 493–508.

Spencer, D.A., Ramsay, J.G., Spencer-Cervato, C., Pognante, U., Ghazanfar, M., Nawaz Chaudhry, M., 1990. High pressure (eclogite facies) metamorphism in the Indian plate, NW Himalaya, Pakistan. Geological Bulletin University of Peshawar 23, 87–100.

Spencer, D.A., Pognante, U., Tonarini, S., 1995. Geochemical and Sr–Nd isotopic characterization of Higher Himalayan eclogites (and associated metabasites). European Journal of Mineralogy 7, 89–102.

Steiger, R., Jaëger, E., 1977. Subcommission on geochronology: convention on the use of decay constants in geo-and cosmochronology. Earth and Planetary Science Letters 36, 359–362.

Treloar, P.J., Potts, G.J., Wheeler, J., Rex, D.C., 1991. Structural evolution and asymmetric uplift of the Nanga Parbat syntaxis, Pakistan Himalayas. Geologisches Rundschau 80, 411–428.

Treloar, P.J., Rex, D.C., Guise, P.G., Wheeler, J., Hurford, A.J., Carter, A., 2000a. Geochronological constraints on the evolution of the Nanga Parbat syntaxis, Pakistan Himalaya. Geological Society, Special Publication, London 170, 137–162.

Treloar, P.J., George, M.T., Whittington, A.G., 2000b. Mafic sheets from Indian plate gneiss in the Nanga Parbat syntaxis: their significance in dating crustal growth and metamorphic and deformation events. Geological Society, Special Publication, London 170, 25–50.

Valley, J.W., O'Neil, J.R., 1981. 13C/12C exchange between calcite and graphite: a possible thermometer in Grenville marbles. Geochim. Cosmochim. Acta. 47, 1527–1530.

Valley, J.W., 1986. Stable isotope geochemistry of metamorphic rocks. Mineralogical Society of America, Reviews in Mineralogy 16, 445–490.

Villa, I., Ruffini, R., Rolfo, F., Lombardo, B., 1996. Diachronous metamorphism of the Ladakh terrain at the Karakorum–Nanga Parbat–Haramosh junction (NW Baltistan, Pakistan). Schweizerische Mineralogische Petrographische Mitterlungen 76, 245–264.

Wadia, D.N., 1933. Note on the geology of Nanga Parbat (Mt Diamir) and adjoining portions of Chilas, Gilgit district, Kashmir. Records of the Geological Survey of India 66, 212–234.

Wada, H., Suzuki, K., 1983. Carbon isotopic thermometry calibrated by dolomite-calcite solvus temperatures. Geochim. Cosmochim. Acta, 47, 697–706.

Winslow, D., Chamberlain, C.P., Zeitler, P.K., 1995. Metamorphism and melting of the lithosphere due to rapid denudation, NPHM Himalaya. Journal of Geology 103, 395–409.

Zeitler, P.K., 1985. Cooling history of the northwest Himalaya, Pakistan. Tectonics 4, 127–151.

Zeitler, P.K., Sutter, J.F., Williams, I.S., Zartman, R., Tahirkheli, R.A.K., 1989. Geochronology and temperature history of the Nanga-Parbat–Haramosh massif, Pakistan. Geological Society of America, Special Paper 232, 1–22.

Zeitler, P.K., Chamberlain, C.P., Smith, H.A., 1993. Synchronous anatexis, metamorphism, and rapid denudation at Nanga Parbat (Pakistan Himalaya). Geology 21, 347–350.